Наносистеми, наноматеріали, нанотехнології
Nanosystems, Nanomaterials, Nanotechnologies
2011, т. 9, № 2, сс. 441–455

PACS numbers: 61.50.Lt, 61.72.Bb, 66.30.-h, 71.15.Nc, 71.20.Be, 73.20.At, 75.75.-c

Interstitial Cr Impurities in Iron: Multiferroic Properties

Z. A. Duriagina, N. Pavlenko*, and N. Shcherbovskikh

Institute for Applied Mathematics and Fundamental Sciences,
Lviv Technical University,
10 Ustyianowycha Str.,
79013 Lviv, Ukraine
**Institute for Condensed Matter Physics,*
1 Svientsitskii Str.,
79011 Lviv, Ukraine

Using the density functional theory, we perform a full atomic relaxation of the bulk ferrite with 12.5%-concentration of monoatomic interstitial Cr, which is periodically located at the edges of the Fe_α b.c.c. cell. As shown, structural relaxation leads to significant atomic displacements and results in the formation of novel high-stable magnetoelastic configurations with parallel chains of octahedrically arranged Fe. The enhanced magnetic polarization in the low-symmetry metallic state of such alloys can be externally controlled by additional introduction of nonmagnetic impurities like nitrogen. The electronic properties of obtained interstitial alloys can have important consequences for the applications in spintronic and multifunctional devices.

З використанням теорії функціоналу густини виконано повну атомову релаксацію об'ємного фериту з 12,5%-концентрацією моноатомового міжвузловинного Cr, який періодично розташовується на гранях ОЦК-комірки Fe_α. Показано, що структурна релаксація призводить до значних зміщень атомів і формування нових високостабільних конфіґурацій з паралельними ланцюжками октаедрично впорядкованого Fe. Збільшена магнетна поляризація в низькосиметрійному металевому стані цього типу стопів може контролюватися ззовні додатковим введенням немагнетних домішок, таких як азот. Електронні властивості одержаних стопів втілення можуть виявитися важливими для їх застосування в спінтроніці та багатофункціональних приладах.

С использованием теории функционала плотности произведена полная атомная релаксация объёмного феррита с 12,5%-концентрацией моноатомного междоузельного Cr, который периодически располагается на гранях ОЦК-ячейки Fe_α. Показано, что структурная релаксация приводит к значительным смещениям атомов и формированию новых высокоста-

бильных конфигураций с параллельными цепочками октаэдрически упорядоченного Fe. Увеличенная магнитная поляризация в низкосимметрийном металлическом состоянии этого типа сплавов может контролироваться извне дополнительным внедрением немагнитных примесей, таких как азот. Электронные свойства полученных сплавов внедрения могут оказаться важными для их применения в спинтронике и многофункциональных приборах.

Key words: metal alloys, Fe–Cr, magnetoelastic effect, atomic implantation.

(Received November 18, 2010)

1. INTRODUCTION

Last years demonstrated an increased activity in search for novel materials where the electronic properties can be altered by inclusion of different atoms or ionic groups. The prominent example is the stainless steels, where the implantation of chromium, molybdenum, nitrogen, and other elements strongly change microstructure of subsurface layers and modify their corrosion and hardness [1].

In search for new efficient multifunctional materials for technological applications in wide series of long-term devices, the properties like hardness, corrosion, heat resistance and other types of mechanical and chemical durability are of central interest [2, 3]. As it frequently appears in science and technology, some well-known materials, when analysed from different points of view and in combination with other compounds, give rise to unexpected features not revealed previously.

As an example of such a new behaviour, in the present work, we discuss a Fe–Cr alloy. Substitutional alloys of Fe with Cr attracted much attention of theory and experiment due to their magnetic properties, and especially due to local antiferromagnetism in the proximity of Cr [4–7]. In our work, we consider different type of alloys, namely, interstitial Fe–Cr alloys where the Cr impurities are located in the interstitial positions of the b.c.c. lattice of Fe_α. The alloys Fe–Cr doped with C, Ni or other compounds are widely used as basic components for ferrite, martensitic and austenitic steels and are responsible for their mechanical and physical properties. In the theoretical studies of the interstitials in Fe–Cr, the different types of the interstitial configurations were previously calculated. Among them, a pair configuration <111> dumbbell is considered as the most energetically favourable, which requires about 4.2 eV for its formation under irradiation [8, 9]. In this work, we analyse monoatomic interstitial configurations with single Cr atoms on the edges of the b.c.c. ferrite. As appears from the calculations of optimized structures, the energy gain for such configurations can approach 6.17 eV that makes this type of interstitial defects especially stable and robust. It should be also noted that the fundamental difference between

the industrial alloys and the alloy studied in the present work is the ordered and periodic character of the latter. In steels, due to their amorphous character, the impurities are distributed randomly. Moreover, the process of the hardening of steels proceeds through the surface treatment and is accompanied by formation of granular microstructure with the changed concentration of impurities and modified properties [10]. In contrast to this, in the systems considered in the present work, the Cr impurities are located periodically in the cubic lattice of Fe_α. Due to substantial local forces, the atomic positions have to be structurally relaxed, which produces patterns with unexpected microstructures and new properties. Last x-ray studies give a direct support of the presence of Cr in the interstitial positions of stainless steels that motivates the studies of interstitial Fe–Cr alloys.

In the present work, we obtain that the optimized lattice microstructure has a clusterized or chain-like character where the chains of octahedrically arranged Fe are parallel arranged along the (001) axis. We show that the competing ferromagnetic and antiferromagnetic interactions lead to spatially inhomogeneous magnetic moments. We also find a significant increase of the magnetization of the structurally relaxed system, which makes the generated systems perspective candidates for spin polarisers in spintronic applications. In the chain-like structures, the relaxation leads to the formation of spatial areas with low carrier density. We suggest that these areas can be considered as channels for the diffusion of light impurities like N, Li, C and others. In a study of the diffusion of nonmagnetic nitrogen in these channels, we calculate diffusion barriers for nitrogen and obtain a strong dependence of the magnetization on N location. Our findings show that the structural relaxation plays a central role and must be inevitably considered in any realistic studies of the considered interstitial alloys.

2. STRUCTURAL RELAXATION OF INTERSTITIAL Fe_α–Cr ALLOY

To study Cr atoms in the interstitial positions of b.c.c. Fe_α, we generated a supercell, which is based on a doubled 2×2 cubic cell of ferrite with Cr located on one of the edges of elementary cubic unit cell (see Fig. 1). In this way, the modelled Fe_8Cr structure is determined as interstitial Fe–Cr alloy with Cr concentration $n = 0.125$ that is typical for stainless steels. The presence of interstitial Cr leads to significant local forces acting on the neighbouring Fe atoms. To minimize these forces, the coordinates of all atoms have been relaxed by the application of the procedure of the minimization of the total energy. The optimization of the supercell has been performed by employing a density functional theory (DFT) implemented using linearized augmented plane wave (LAPW) method in the full potential Wien2k code [11]. It is known that the Cr impurities perturb the antiferromagnetic surrounding of Fe_α in the

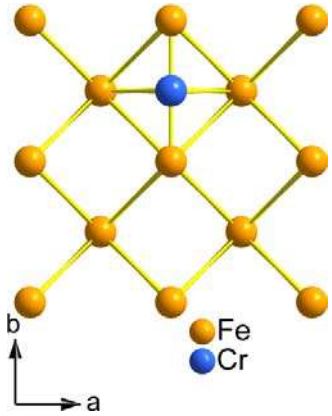

Fig. 1. Schematic view of unrelaxed Fe containing 12.5% of interstitial Cr.

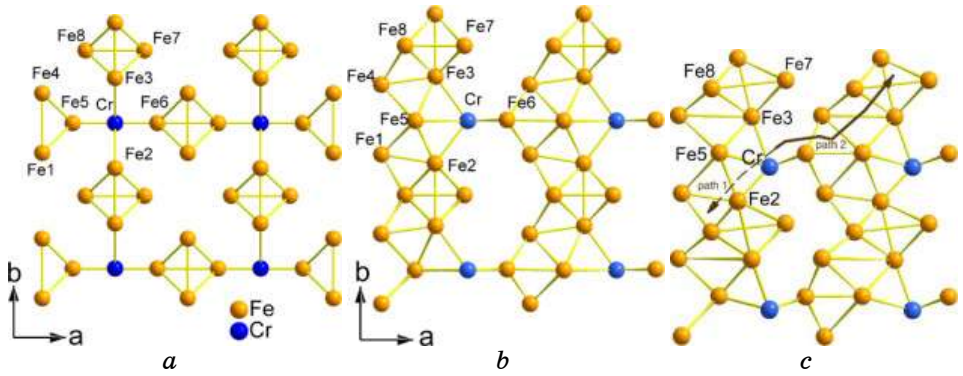

a *b* *c*

Fig. 2. Relaxed structure of Fe with 12.5% of Cr: (*a*) LDA calculations; (*b*) spin-polarized LSDA calculations in the structure with $a = b = 2.86$ Å; (*c*) spin-polarized LSDA calculations in the structure with $a = b = 3.0$ Å. The path 1 and path 2 identify possible paths for diffusion through the channels formed due to atomic relaxation.

substitutional alloys. Therefore, to study the effect of spin polarization, two different relaxation approaches have been employed. In the first approach, the atomic optimal positions were calculated in the local density approximation (LDA) on a 2×2×5 **k**-points grid. In the second procedure, to consider the states with different spin orientations, we have optimized the structure by employing a local spin density approximation (LSDA). The results of both methods of the structural relaxation are represented in Fig. 2.

The central feature, which is commonly present after performing both LDA and spin polarized-optimization, is the clusterization of the sublattice of iron atoms. In the LDA-optimized structure (Fig. 2, *a*), the

clusterization leads to the formation of a high-symmetry network. In the (x, y) (or a, b) planes, this network consists of Fe_6 octahedra in the middle of the edges of tetragonal unit cell which are connected to the neighbouring iron octahedron of the opposite edges by the Fe–Cr bonds of the length 1.9 Å. It is worth noting that despite the significant displacements of iron atoms, the net electric polarization of the cell is zero due to high structural symmetry $C4/m$ remaining after the relaxation. The formation energy of the relaxed Fe_8Cr configuration can be calculated as $E_f(\text{LDA}) = E_{tot}(Fe_8Cr) - 8E_{tot}(Fe) - E_{tot}(Cr)$, where the last two terms are the total energies of bulk b.c.c. Fe_α and Cr respectively. For the bulk Fe_α, we used the energy value obtained in the ferromagnetic state, whereas the total energy of bulk Cr has been calculated for a non-magnetic system. With these values, we find that $E_f(\text{LDA}) = 4.82$ eV. In a similar way, we calculated the energy $E_f(\text{unrlx})$ of the formation of initial unrelaxed configuration, which is equal to 5.02 eV. Therefore, the significant energy gain due to the structural relaxation, $\Delta E(\text{LDA}) = E_f(\text{unrlx}) - E_f(\text{LDA}) = 0.196$ eV, shows a central importance of the atomic displacements for the stability of the considered systems.

In the LDA-optimized structure, the spin-polarized calculations lead to the local magnetic moment for Cr: $Fe_{Cr} = -0.23Fe_\alpha$, which is of the opposite sign to the moments of Fe atoms. In the relaxed cell, iron atoms the most distant from Cr have the bulk magnetic moment of $1.7Fe_\alpha$. In distinction from this, the magnetic moments of Fe in the close vicinity of Cr are substantially suppressed to the values of $0.97Fe_\alpha$. As a result, the appearing spatial magnetic pattern is strongly inhomogeneous and contains the antiferromagnetic regions near Cr separated by ferromagnetically ordered Fe atoms. The obtained significant suppression of the Fe moments close to Cr is in contrast to the substitutional Fe–Cr alloys for which the LSDA approach gives almost homogeneous values of all Fe moments in the range of $2.65–2.85Fe_\alpha$. In this case, for the magnetic moment of Cr, we obtain $Fe_{Cr} = -2.93Fe_\alpha$.

In distinction to the LDA relaxation, the LSDA optimization procedure produces completely new ordered structural patterns shown in Fig. 2, *b* and Fig. 2, *c* for two different (unrelaxed, $a = b = 2.86$ Å, and relaxed, $a = b = 3$ Å) lattice constants. The last structure (*c*) corresponds to the 13%-increase of the unit-cell volume due to the insertion of the interstitial Cr. In these two cases, the optimized structural pattern is characterized by the chains of atomic groups along the x (a) direction where each group contains six Fe atoms. The obtained chains are parallel arranged along the x axis with the distance of about 4 Å between the Fe atoms in the neighbouring chains and are connected to each other by the Fe–Cr bonds with the length of about 2.4 Å, for the structure (*b*) with $a = 2.86$ and 2.7 Å, for the structure (*c*) with relaxed $a = 3.0$ Å. The local antiferromagnetic ordering is characterized by the magnetic moments $\mu_{Cr} = -0.72\mu_B$, $\mu_5 = 2.4\mu_B$, and $\mu_6 = 1.25\mu_B$ of the neighbouring atoms Fe_5

and Fe_6 respectively. The magnetic moments of the more distant iron atoms have the values around $2.5\mu_B$, which is close to values found in substitutional alloys and in pure iron [8].

As compared to the tetragonal structure of the LDA-optimized system, the chain-like structure of the LSDA-relaxed supercell is characterized by substantially lower crystal symmetry and by the absence of the inversion centre. The formation energy of the LSDA-relaxed Fe_8Cr configuration, $E_f(\mathrm{LSDA}) = E_{tot}(Fe_8Cr) - 8E_{tot}(Fe) - E_{tot}(Cr) = -1.15$ eV, is well below the energy $E_f(\mathrm{LDA})$ of formation of the LDA configurations. We can also calculate the energy gain due to the structural relaxation by the LSDA approach, $\Delta E(\mathrm{LSDA}) = E_f(\mathrm{unrlx}) - E_f(\mathrm{LSDA}) = 6.17$ eV, which demonstrates a high stability of the relaxed spin-polarized structure.

In the considered systems, we also analysed the dependences of the local magnetic properties on the interatomic distances. To see how the atomic displacements affect magnetic moments of surrounding atoms, in Fig. 3, we show the local moments of Cr and of two nearest neighbouring Fe as a function of the Cr displacement $\Delta = x(\mathrm{Cr}) - x(Fe_5)$ between Fe_5 and Fe_6 along the x axis. The increase of Δ leads to the change of μ_{Cr} from $-0.7\mu_B$ to the value of about $-0.73\mu_B$. On the other hand, the larger Δ and the resulted elongation of the [Fe_5–Cr] bond leads to the reduced $\mu_5 = 2.39\mu_B$, which implies a tendency for the suppression of antiferromagnetism near Fe_5. In contrast to this, the increase of Δ produces the enhancement of μ_6 from $1.25\mu_B$ to the values of about 1.28–$1.3\mu_B$, an opposite trend, which occurs with the shortening of the bond between Cr and Fe_6.

In Figure 3, the negative Δ leads to the changes of magnetic mo-

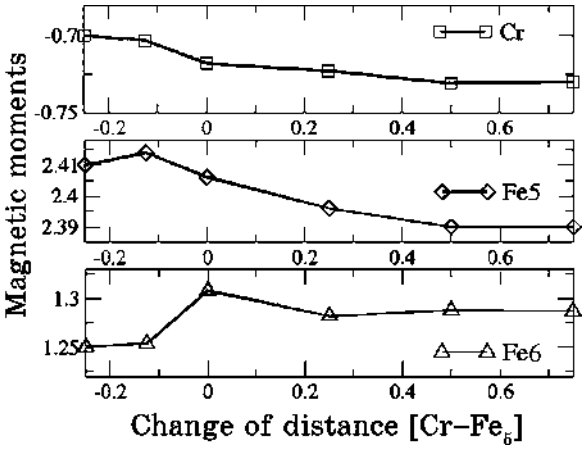

Fig. 3. Local magnetic moments of the atoms in Fe_5–Cr–Fe_6 triad versus the displacement $\Delta = [Fe_5\text{–Cr}] - [Fe_5\text{–Cr}]^0$ of Cr along the (100) axis. Here, $[Fe_5\text{–Cr}]^0$ is the equilibrium distance between Fe_6 and Cr.

ments, which are strongly asymmetric to the corresponding changes at $\Delta > 0$. Consequently, the obtained magnetoelastic coupling produces the anisotropy of the magnetic moments and is accompanied by the loss of the inversion centre due to the atomic displacements—an effect, which can be observed in Fig. 2, *b* and *c*. In Figure 2, *c*, the low-symmetry structure corresponds to the minimum of the total energy. In Figure 2, *a*, a principally different high-symmetry structure appears from the relaxation of structural degrees of freedom in the spin-unpolarized structure. In view of this, the neglecting of the magnetoelastic coupling in electronic structure calculations does not allow to achieve a full relaxation in this-type interstitial alloys.

Figure 4 shows the valence 3*d* electron density contours in the (*x*, *z*) planes, which are plotted for the spin-up and spin-down magnetically polarized states. One can see that the majority 3*d* spin-up states of Fe

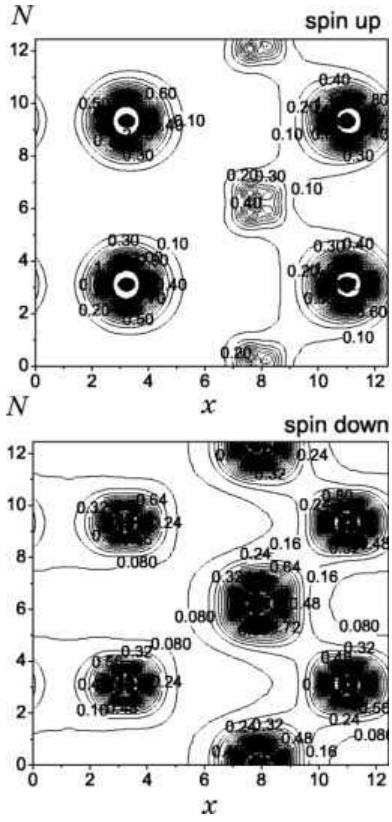

Fig. 4. Contours of electron density maps in the (*x*, *z*) plane ($y/b = 0.25$, *x* and *z* given in Å) obtained by integration of electronic states in the energy window *E* between –3 eV below the Fermi level and the Fermi level. The results obtained by the structural optimization using the LSDA approximation.

are highly occupied by electrons, whereas the electron concentration of Cr spin up states is substantially lower. The opposite effect with high electron occupation of Cr and lower electron density on Fe is obtained for the spin-down electrons. The chain-like structures Fe–Cr observed in this case in the z direction result in strong hybridization between the intrachain $3d$ spin-down orbitals of Fe and Cr. The last feature leads to the spatial charge redistribution and to higher charge densities on the bonds between spin-down Cr and Fe. In the LSDA-optimized system, the structural optimization produces areas with low charge density in the y (b) direction, where each area can be identified between the chains of Fe octahedron. As can be seen in Fig. 4, these areas are almost free of charge and can be considered as channels for the diffusion of light atoms like H, Li or N.

Figure 5 presents the density contours calculated for the LDA-

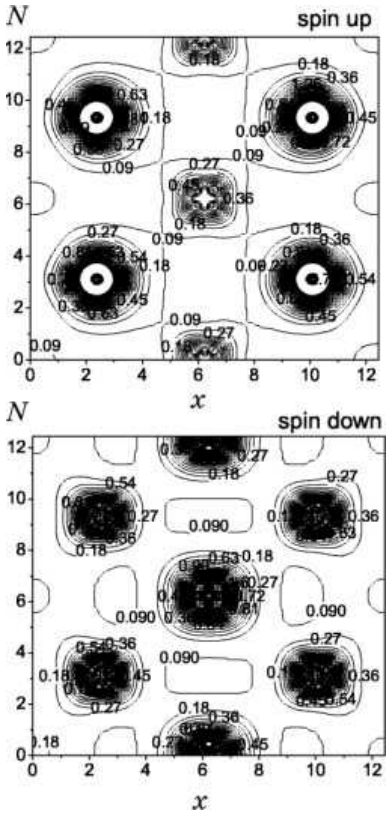

Fig. 5. Contours of electron density maps in the (x, z) plane ($y/b = 0.25$, x and z given in Å) calculated by integration of electron states in the energy window E between –3 eV below the Fermi level and the Fermi level. The LSDA results obtained in the initially LDA-relaxed structure.

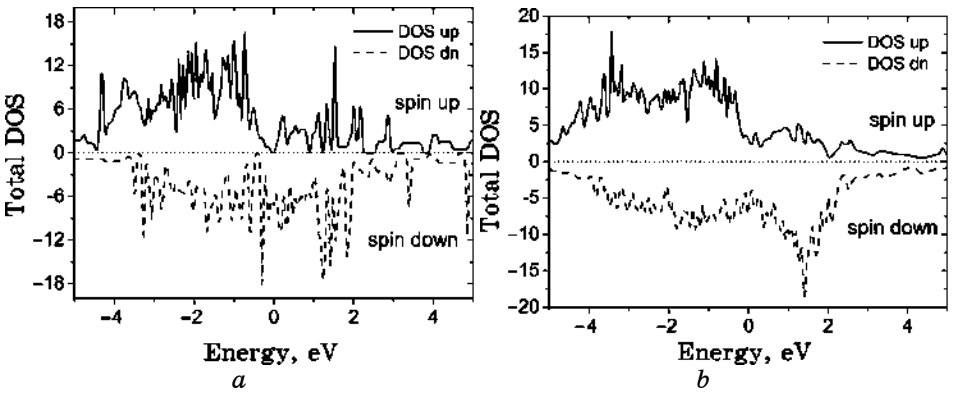

Fig. 6. Total density of states for structures optimized using (*a*) LDA approach and (*b*) spin-polarized LSDA approximation. The Fermi level corresponds to $E = 0$.

optimized structure. Similarly to the contours in Fig. 4, the electron density of the majority Fe and Cr orbitals and on the bonds between Cr and Fe is substantially lower than the charge density on the spin-down contours, although the spatial charge distribution is more homogeneous as compared to that in Fig. 4.

For the LDA-relaxed structure, the density of states is characterized by a strong suppression of the majority spin-up DOS near the Fermi level (Fig. 6, *a*). In contrast, the minority spin-down DOS exhibits significant values at the Fermi level. Similar, although much stronger, suppression of majority DOS is typically observed in half-metallic systems where the electric current is conducted by electrons with the same direction of spin [12]. In contrast to the half-metallic-like features of the high-symmetry alloys, the DOS for the LSDA-optimized system (Fig. 6, *b*) demonstrates substantial values at the Fermi level for both spin directions, which implies an enhancement of the metallic state for the majority electrons. Such an enhancement occurs due to the significant atomic distortions, which are in the range from $\Delta R_i = 0.2$ Å ($i = 3$, Fe_3 in Fig. 2) to $\Delta R_i = 0.84$ Å ($i = 0$, Cr in Fig. 2) in the low-symmetry structure.

In the transition metal oxides, the metallic state obtained by the LDA method frequently disappears by the additional account for the local Coulomb corrections for the electrons of *d* orbitals [13, 14]. In our work, the Coulomb corrections are taken into account within the SIC variant of the LSDA + U approximation introduced in Ref. [13]. The results are presented in Fig. 7 for two different values of $U = 2$ eV and $U = 4.5$ eV estimated and employed in Refs. [15–17] for the electron repulsion of charge of 3*d* orbitals of Fe and Cr. One can clearly see that despite the significant Coulomb corrections, the metallic state mani-

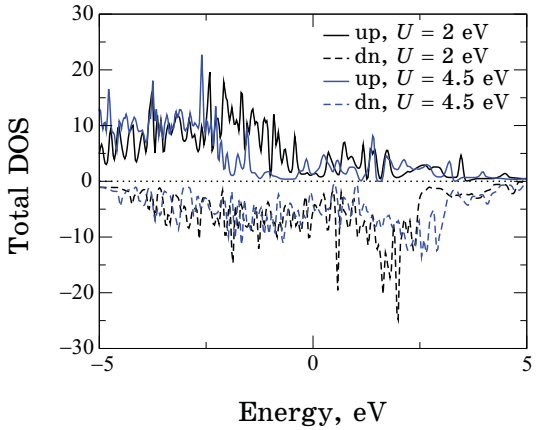

Fig. 7. Total densities of states for the LSDA-optimized structure calculated by the LSDA + U method with the local Coulomb corrections for the 3d orbitals of Fe and Cr U = 2 eV ('black' curves) and 4 eV ('blue' curves). The Fermi level corresponds to $E = 0$.

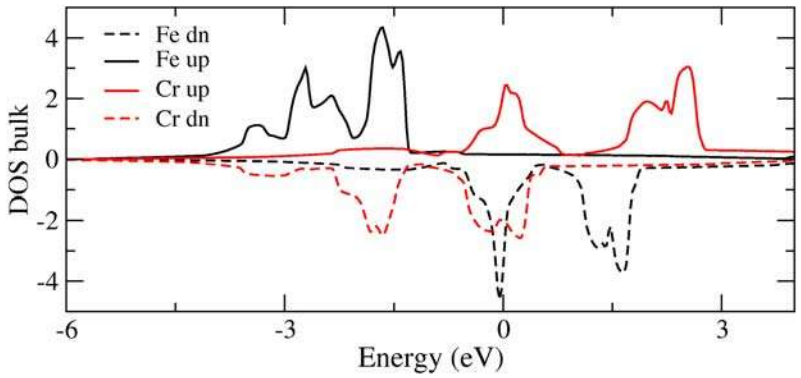

Fig. 8. Total densities of states for bulk Cr and Fe. Here, the Fermi level corresponds to $E = 0$.

fests itself by a finite density of states at the Fermi level corresponding to $E = 0$. The close examination of the DOS of bulk Fe and Cr in Fig. 8 shows that the origin of the metallic state is in the conducting 3d charge of Cr, which becomes highly hybridized with the 3d orbitals of Fe due to the atomic distortions in the structurally relaxed interstitial alloy. This explains why the metallic state of the considered Fe–Cr alloy appears to be a sustainable macroscopic property.

Although the LSDA-optimized structure is characterized by the disappearance of the majority energy gap, the cell magnetic moment, $M_{\mathrm{LSDA}} = 3.84\mu_B$, is larger than the magnetic moment in the LDA-

optimized cell, $M_{\mathrm{LDA}} = 2.88\mu_B$. Such an enhancement of the magnetic polarization is caused by the increase of electric polarization and should be considered as a direct evidence of the strong magnetoelastic effect, *i.e.*, the increase of M due to the distortions, ΔR_i. It is remarkable that, in the substitutional alloy Fe–Cr with 12.5% of Cr, the LSDA approach gives a value of $3.8\mu_B$ for the cell magnetic moment, which is slightly lower than the magnetic moment for the considered LSDA-relaxed substitutional alloy.

The obtained high spin polarization of the interstitial Fe–Cr alloys allows us to suggest these materials as possible candidates for spin polarisers in the spintronic devices. Another question related to the stability of the considered interstitial alloys is how other kinds of atomic impurities can modify the electronic properties. In the structurally relaxed system, the location of the light impurity atoms like N or Li is expected to be mainly restricted to the channels discussed above and observed in Fig. 4. Therefore, the diffusion of the impurities should be considered in the context of possible diffusion paths within the channels formed in Fe_α due to atomic distortions.

3. DIFFUSION PATHS OF N IN INTERSTITIAL Fe_α–Cr ALLOYS

It is worth noting that the distortions due to the atomic relaxation produce well-defined diffusion channels along the (001) direction. In two different configurations shown in Fig. 9, such a channel contains one atom of N. The top picture presents an example of N on the boundary surface of the cubic cell with $z_{\mathrm{N}} = 0$, whereas the bottom picture demonstrates a configuration with N ($z_{\mathrm{N}} = 0.5c$) located inside the cell. Therefore, the diffusion paths of N contain two stages: (i) the intracell stage with the migration of N within the cell and (ii) the intercell stage, which combines the diffusion of N near the boundaries of the cells and the crossing of these boundaries.

To study the diffusion process in the channel, we consider first the relaxed structure of Fe–Cr alloy, which does not contain additional impurities like nitrogen. In the relaxed structure with the channels appeared due to atomic distortions (Fig. 2, *c*), we choose an interstitial position for N at the cell boundary (position (VI) indicated in Fig. 10) and perform the full LSDA optimization of the generated Fe–Cr–N ternary alloy. In this way, by continuous relaxation of the surrounding due to the migration of N, we can study the diffusion paths and the activation energies for the migration of N atoms through the alloy. The results of the full relaxation of the surrounding are presented in Fig. 9 in the two snapshots of the cell atomic structure. In these pictures, modifications of the position of N due to the migration are accompanied by additional distortions of the neighbouring Fe and Cr.

The examples of the diffusion paths 1 and 2 formed by the motion of

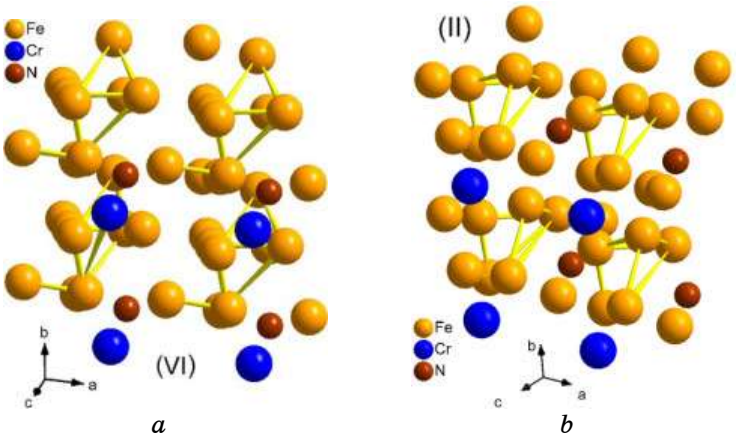

Fig. 9. Two different cases of structure relaxation due to migration of nitrogen in the channel of the optimized crystal cell of Fe–Cr. The left picture represents the location of N on the boundary of the cell with $z = 0$, and in the right structure, N at $z = 0.5c$ is located inside the unit cell.

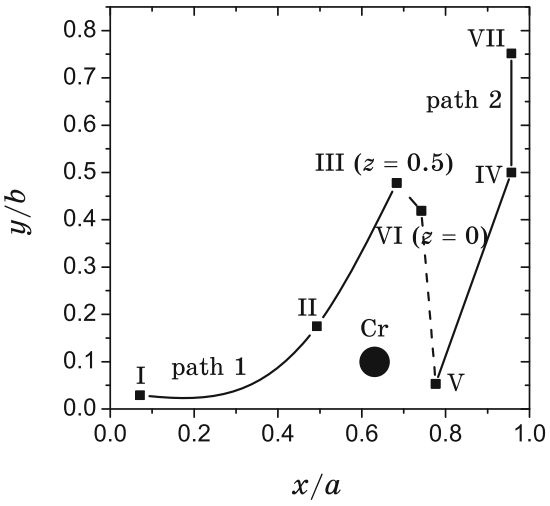

Fig. 10. Schematic paths of the migration of N inside the conducting channel. Here, the positions I–III–VI on the face $z = 0$ of the unit cell correspond to the migration of N along the path 1 shown in Fig. 2, *c*. The positions VI–V–IV–VII ($z = 0.5c$) identify the diffusion of N inside the channel along path 2.

N between different positions (I, II, III, IV, V, VI) are schematically shown in Fig. 2, *c* and are presented in details in Fig. 9 in projection on the (x, y) plane.

To analyse the diffusion mechanism along different paths, two types

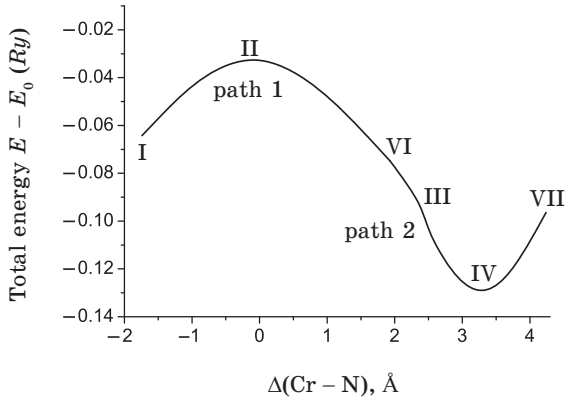

Fig. 11. Total energy of the system versus the distance Δ from Cr to N. Here, the positive and negative Δ correspond to the diffusion along the path 1 and path 2, respectively. The symbols I–VII identify the location of N on these paths.

of the locations of N have been selected: (i) position VI on the boundary $z = 0$ close to Cr and (ii) the internal positions I–II–III and VI–V–IV–VII with $z = 0.5c$, which corresponds to two different directions (path 1 and path 2) of the migration of N inside the channels of the unit cell. Using the procedure of the structural relaxation described above for each considered fixed position k = I–VII for N, we have calculated the expenditure of energy, $\Delta E_{kl} = E_k - E_0$, for the migration of N. In the definition of ΔE_{kl}, E_k is the total energy of the relaxed system with N fixed in the position k, whereas E_0 is the energy of the initial configuration (position VI in Fig. 10). The results in Fig. 11 show the presence of the energy barrier of about $\Delta E_c = 1.3$ eV, which must be overcame at the migration of N from the vicinity of Cr inside the channel. The obtained value is in sufficiently good agreement with the recent experimental findings, which report an activation energy in the range from 1.7 eV to 0.8 eV for the diffusion of nitrogen in stainless AISI steels [17].

The question, which arises due to the inclusion of N into the Fe–Cr alloy, is how the N impurities modify the magnetic properties of the system. Figure 12 presents the change of the total magnetic moment of the cell during the migration of N along path 1 and path 2 identified in Fig. 10. Although the nitrogen is initially nonmagnetic in the bulk, it becomes magnetic near the Cr–Fe complex with a small magnetic moment of $-0.04\mu_B$ induced by the magnetism of the surrounding. It is noteworthy that the total magnetic moment of the cell is also increased when N is located near Cr. Such an increase is explained by the strong additional distortions in the range from 0.04 Å (Fe_7) up to 0.2 Å (Fe_3) caused by the migration of N. Like in the pure Fe–Cr, such extra distortions lead to the increase of magnetic polarization due to magnetoelastic effect.

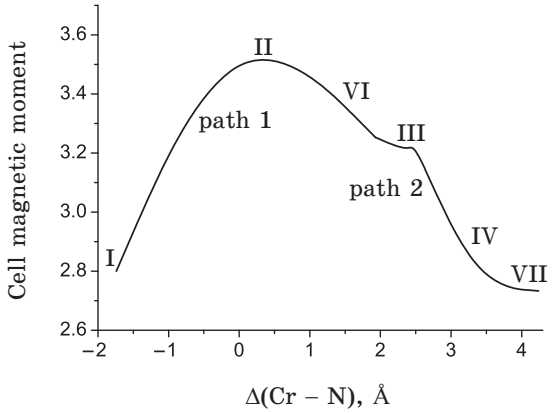

Fig. 12. Total cell magnetic moment versus the distance Δ from Cr to N. Here, the positive and negative Δ correspond to the diffusion along path 1 and path 2, respectively. The symbols I–VII identify the location of N on these paths.

In Figure 12, the increase of the distance to Cr leads to suppression of the magnetic moment of N and to decrease of the total magnetic polarization within the cell to the values obtained for LSDA-relaxed Fe–Cr alloys. The obtained drastic change of the magnetic polarization clearly demonstrates a crucial importance of the location of nonmagnetic impurities like N for the electronic properties of alloy. As follows from our findings, a possible control of the location of N, for example, by external electric field, can lead to externally controlled changes of the magnetic polarization—a feature, which is of crucial importance for the spintronic devices.

4. CONCLUSION

We have shown that the full atomic relaxation of the bulk ferrite with 12.5% concentration of interstitial Cr stabilizes new chain-like structure of lower symmetry. In this structure, the monoatomic Cr in the edges of ferrite b.c.c. cells leads to the local atomic distortions and results in the formation of parallel-aligned chains of Fe_6 octahedrons, which are connected by the interchain Fe–Cr bonds. The energy gain caused by such a structural relaxation approaches 6.17 eV, which makes this-type interstitial alloy highly stable and energetically favourable with the negative formation energy approaching –1.15 eV. The novel electronic state of the system can be characterized as metal, where the metallic properties are the result of high Fe–Cr hybridization of the structurally relaxed alloy. In the investigations of the magnetic state of the generated relaxed structures, we have obtained a local antiferromagnetic order in the close proximity of Cr atoms, where-

as the more distant Fe atoms are coupled ferromagnetically. As a result, in the obtained chain-like structure, the atomic distortions lead to the formation of the metallic state with high magnetic polarization. We have also shown that the nonmagnetic impurities like nitrogen can substantially modify the magnetic properties of the interstitial alloy, which can be considered as an additional manifestation of the strong magnetoelastic effect in this type of multiferroics. We suggest consideration of the generated interstitial alloys as perspective candidates for future applications in spintronic and multifunctional devices.

ACKNOWLEDGEMENTS

This work has been partially supported through the project 'Models of quantum statistical description of catalytic processes on metallic substrates' of the Ministry of Education and Sciences of Ukraine and the grant 0108U002091 of the National Academy of Science of Ukraine.

REFERENCES

1. D. Peckner and I. M. Bernstein, *Handbook on Stainless Steels* (New York: McGraw-Hill Book Co: 1977).
2. A. Mai, V. A. C. Haanappel, S. Uhlenbruck, F. Tietz, and D. Stover, *Solid State Ionics*, **176**: 1341 (2005).
3. H. Yokokawa, H. Tu, B. Iwanschitz, and A. Mai, *J. Power Sources*, **182**: 400 (2008).
4. R. H. Victora and L. M. Falicov, *Phys. Rev. B*, **31**: 7335 (1985).
5. A. T. Paxton and M. W. Finnis, *Phys. Rev. B*, **77**: 024428 (2008).
6. C. Paduani and J. C. Krause, *Braz. Journ. of Physics*, **36**: 1262 (2006).
7. A. Davies, J. A. Stroscio, D. T. Pierce, and R. J. Celotta, *Phys. Rev. Lett.*, **76**: 4175 (1996).
8. T. P. C. Klaver, P. Olsson, and M. W. Finnis, *Phys. Rev. B*, **76**: 214110 (2007).
9. P. Olsson, C. Domain, and J. Wallenius, *Phys. Rev. B*, **75**: 014110 (2007).
10. Z. A. Duriagina and M. I. Pashechko, *Metal Science and Treatment of Metals*, **4**: 34 (2000).
11. P. Blaha, K. Schwarz, G. K. H. Madsen, D. Kvasnicka, and J. Luitz, *WIEN2k: An Augmented Plane Wave + Local Orbitals Program for Calculating Crystal Properties*, ISBN 3-9501031-1-2 (Wien: TU Wien: 2001).
12. J.-H. Park et al., *Nature*, **392**: 794 (1998).
13. V. I. Anisimov, I. V. Solovyov, M. A. Korotin, M. T. Czyzyk, and G. A. Sawatzky, *Phys. Rev. B*, **48**: 16929 (1993).
14. M. T. Czyzyk and G. A. Sawatzky, *Phys. Rev. B*, **49**: 14211 (1994).
15. T. Bandyopadhyay and D. D. Sarma, *Phys. Rev. B*, **39**: 3517 (1989).
16. Ze Zhang and S. Satpathy, *Phys. Rev. B*, **44**: 13319 (1991).
17. M. A. Korotin, V. I. Anisimov, D. I. Khomskii, and G. A. Sawatzky, *Phys. Rev. Lett.*, **80**: 4305 (1998).
18. L. F. Zagonel, C. A. Figueroa, R. Droppa, Jr., and F. Alvarez, *Surface and Coatings Technology*, **201**: 452 (2006).